e-Navi

Available online at http://www.e-navi.kr/
e-Navigation Journal

Original article

# Treatment of Ship Ballast Water by Biomimetic Electric Ray TENG

Youzhi Wang[a*]

[a] Management School, Hainan University, Haikou 570228, China

## Abstract

This study explores the innovative utilization of a biomimetic electric ray friction nanogenerator (ER-TENG) in combination with electrolysis technology for the remediation of maritime effluent. The ER-TENG is ingeniously crafted with a flexible, planar structure, enabling seamless adaptation to various curved and irregular substrates such as rocks, corals, and shipwrecks on the ocean floor, obviating the necessity for specialized mounting or securing devices. Simulation results regarding the potential distribution between the copper electrode and the PDMS film under different inter-electrode distances indicate that an increase in separation distance is correlated with an enhanced potential difference on the material's surface, exhibiting a linear upward trend, with the maximum potential difference reaching 120 V. When TiO2 nanoparticles are incorporated at a doping mass fraction of 4.65 wt%, the friction nanogenerator attains its peak electrical performance, boasting a peak open-circuit voltage of 123.25 V and a maximum short-circuit current of 13.52 μA, representing increases of 2.73-fold and 2.56-fold in open-circuit voltage and short-circuit current, respectively. At operational frequencies of 1.2 Hz and 1.0 Hz, the initial stage of sterilization rate enhancement proceeds at a moderate pace. However, after 60 minutes of electrolysis, sterilization rates reach 88.12% and 46.36%, respectively. The electrical energy harvested by the ER-TENG facilitates the generation of potent oxidizing chlorine through electrolysis, which effectively eliminates harmful aquatic organisms and pathogens present in ship ballast water.

*Keywords: Ballast Water, Electric Ray, Friction Nanogenerator*


https://doi.org/10.52820/j.enavi.2024.23.026

## 1. Introduction

Triboelectric Nanogenerator (TENG) represents a groundbreaking innovation in the realm of energy conversion, harnessing the principles of frictional electrification and electrostatic induction to transmute mechanical energy into electrical energy. In recent years, the profound exploration of bioelectric phenomena in nature has galvanized scientists to emulate these biological mechanisms, paving the way for novel energy harvesting technologies. Among marine organisms, the electric ray stands out for its ability to generate potent electric currents, offering a unique paradigm that inspires the development of biomimetic electric ray frictional nanogenerators.

The operational principle of the biomimetic electric ray frictional nanogenerator hinges upon the frictional electrification effect and electrostatic induction. When two disparate material surfaces engage in contact and subsequently disengage, a charge transfer ensues, attributed to the variance in their electronegativity [1]. This interaction engenders positive and negative charges on the surfaces, establishing a potential difference across the external circuit that propels electron flow and, consequently, generates an electric current. By mimicking the structural intricacies of the electric ray's power-generating organ, the biomimetic electric ray frictional nanogenerator is ingeniously engineered to efficiently capture mechanical energy and convert it into electrical energy.

Since its inception in 2012, TENG has emerged as an avant-garde technology for energy capture and self-powered sensing [2]. TENG leverages the synergistic effects of contact electrification and electrostatic induction to adeptly transform uncontrolled, dispersed, and latent mechanical energy into usable electrical energy. Its foundational mechanism unfolds in two stages: initially, two surfaces make contact and accrue charge through their interaction; subsequently, the motion of these charged surfaces induces current and voltage via electrostatic induction. TENG is distinguished by its cost-effectiveness, structural simplicity, lightweight design, high efficiency in energy utilization, and the versatility of material choices [3,4].

TENG has garnered significant attention in the realm of blue energy harvesting, primarily due to their adaptable architectures and aptitude for activation by low-frequency stimuli [5,6]. In 2024, Li et al. [8] introduced an innovative apparatus that synergistically integrates vortex-induced vibration (VIV) with a multi-growing TENG to harness energy from sluggish ocean currents. This ingenious device operates via an oscillating float, which actuates the TENG, thereby transmuting kinetic energy into electrical energy. Empirical evidence reveals that this system can achieve a peak average power output of nearly 20 μW, particularly when configured with eight grating TENGs. In the same year, Ying Lou et al. [8] unveiled a clamp-structure pendulum-coupled nanogenerator integrated with a dual-track circuit, devised to ameliorate the suboptimal energy conversion endemic to TENGs employed in oceanic monitoring. The spatial efficiency of the CP-CNG architecture can reach an impressive 91.9%. Furthermore, Shuqin Zhang et al. [9] proposed a TENG predicated on the coupling of an asymmetrical array of triboelectric units and electrodes, augmented by a mechanical switch design. Shaojun Zhang et al. [10] conceptualized a biomimetic electric eel TENG designed for the extraction of wave energy, which was subsequently applied to the anti-pollution treatment of ship ballast water. In 2024, Mohamed Salman et al. [11] conducted an insightful exploration of the evolutionary trajectory of wave energy harvesting technologies utilizing TENGs, elucidating both the prevailing challenges and the promising future prospects within this cutting-edge domain. Kushal Ruthvik Kaja et al. [12] have illuminated the potential of the liquid-solid TENG as a formidable alternative, particularly adept at harnessing mechanical energy from aqueous environments. The work of Ming Yuan et al. [13] has yielded remarkable findings, demonstrating a staggering 2220% augmentation in the output voltage of the TMM-TENG when juxtaposed with traditional methodologies. Concerning acoustic energy harvesting, at a sound pressure level of 95 dB, the TMM-TENG achieves a peak-to-peak output voltage of 500 V. Hao Wu et al. [14] present that the harvester can generate a maximum average output voltage of approximately 39.26 V and an instantaneous power of 6.49 μW under excitation conditions of 0.7 Hz frequency and 90 mm amplitude

at an initial water level of 30 mm. Arunkumar Chandrasekhar's [15] work on the smart maracas exemplifies the transformative potential of TENGs in converting mechanical motion into viable electrical energy through precise engineering, thus paving the way for autonomous power solutions across diverse applications.

Ships require the injection of seawater as ballast to ensure safe and stable navigation across the world's oceans. However, the introduction of invasive aquatic species and the physicochemical characteristics of ballast water pose one of the most significant threats to the marine environment, potentially leading to severe ecological, economic, and public health repercussions [16]. The discharge of ballast water often contains a diverse array of biological entities, including plants, animals, viruses, and bacteria. The dissemination of diseases such as paralytic shellfish poisoning and cholera outbreaks can jeopardize human health [17]. This article explores the utilization of ER-TENG in conjunction with electrolysis technology to simulate the prevention of ship ballast water pollution through the electrolysis of seawater. The electrolytic seawater antifouling technology employs specially designed electrodes to electrolyze seawater, generating effective chlorine species, including hypochlorous acid (HClO), hypochlorite ions ($ClO^-$), and chlorine gas ($Cl_2$). Effective chlorine, a potent oxidant, is capable of eliminating the larvae or spores of marine organisms, thereby thwarting their attachment and proliferation.

During the electrolysis process, the anode reaction yields chlorine gas, while the cathode reaction produces hydrogen gas and hydroxide ions. The chlorine gas subsequently reacts with hydroxide ions to form hypochlorite, which exhibits strong oxidizing properties. The electrolytic seawater antifouling technology boasts several advantages, including high efficiency, environmental sustainability, and the absence of chemical residues, making it a crucial component in the ballast water treatment process.

By integrating ER-TENG with electrolysis technology, this study has successfully achieved effective antifouling treatment of simulated ship ballast water. The production of effective chlorine during seawater electrolysis is meticulously controlled, ensuring the eradication of the majority of harmful aquatic organisms and pathogens present in the ballast water. In the simulation experiments, the biological content of the ballast water treated with the combined ER-TENG and electrolysis technology was markedly reduced, meeting the discharge standards set by the International Maritime Organization.

This research offers an innovative and efficacious solution for the antifouling treatment of ship ballast water through the synergistic application of ER-TENG and electrolysis technology. This approach not only excels in terms of high efficiency, environmental protection, and the absence of chemical residues but also facilitates real-time treatment of ballast water, thereby mitigating pollution to the marine environment. With further advancements and optimization of the technology, this solution holds promise for widespread adoption and promotion in the realm of ship ballast water antifouling treatment.

## 2. Reagents and materials

The materials and reagents employed in this experiment encompass analytically pure yeast paste sourced from Tianjin Dingshengxin Chemical Co., Ltd.; analytically pure tryptone, supplied by Qingdao Haibo Biotechnology, which serves as a vital nitrogen source in microbial cultivation and fermentation processes; and analytically graded sodium chloride, a commonly utilized reagent, from Shuangshuang Chemical Co., Ltd. Regarding electronics and electrical components, industrial-grade wires from Xinyicheng Technology Co., Ltd. are incorporated. Industrial-grade acrylic sheet (PMMA) from Jinyi Organic Glass Products Factory is also utilized. Industrial-grade paper from Hobby Production Factory is employed. The industrial-grade rectifier bridge from Chaohe Electronic Appliances is a crucial component in power circuits, adept at transforming alternating current into direct current.

## 3. ER-TENG seawater electrolysis

### *3.1 Selection of electrode materials*

The electrocatalytic performance of electrode materials is pivotal to the efficacy of electrochemical reactions and the efficient harnessing of electrical

energy. In the selection of cathodic materials, it is imperative to prioritize those that can augment electrocatalytic efficiency and selectivity for targeted reactions. In this experimental setup, the hydrogen evolution reaction was facilitated at the cathode, with low carbon steel being chosen as the cathodic material. This material is characterized by its low hydrogen evolution overpotential, cost-effectiveness, ease of fabrication, and operational stability, which provides cathodic protection and resistance to corrosion. Carbon, a non-metallic element, boasts a storied legacy in electrochemical applications dating back to the mid-20th century. Its superior electrical and thermal conductivity, remarkable corrosion resistance, ease of processing, and affordability have rendered it a staple in the electrochemical industry. Taking into account the redox potential of chloride ions and the electrolysis potential of water, carbon rods (10 mm in diameter, 150 mm in length), carbon plates and carbon fiber materials (150 mm in length, 100 mm in width, 2 mm in thickness) were employed as anodes for the treatment of seawater in this experiment.

### *3.2 AC/DC Conversion of ER-TENG*

In accordance with the operational principles of frictional nanogenerators, these devices produce an alternating current (AC), which is inherently unsuitable for directly powering electrolytic reactions. Consequently, in practical applications, it becomes imperative to transform this alternating current into direct current (DC) to facilitate such reactions. The prevalent approach involves the integration of rectifier circuits to transmute the alternating current produced by frictional nanogenerators. During this rectification process, it is essential to connect a rectifying diode in a bridge configuration to the frictional nanogenerator apparatus. The external rectification assembly comprises a frictional nanogenerator, a rectification circuit, a capacitor, and an LED. In the absence of a rectifier circuit, the output current exhibits a sinusoidal waveform. However, once processed through the rectifier bridge, all current values are rendered positive. A comparative analysis of the positive peak values in both scenarios reveals that the output current post-rectification is diminished relative to its pre-rectification state. This attenuation is attributable to the load resistance introduced by the rectifier bridge, which subsequently diminishes the amplitude of the output current.

### *3.3 Determination of sterilization rate*

In the realm of marine ecosystems, bacteria constitute a vital component of the microbial milieu and are a critical focus in the processes concerning the treatment of ship ballast water. This investigation targeted Escherichia coli and Staphylococcus aureus as the subjects of study. These bacterial strains were procured from the Shandong Provincial Key Laboratory of Ship Safety and Pollution Prevention, utilizing the LB (Luria Bertani) medium as the cultivation substrate. The primary constituents of LB medium comprise 5 g/L yeast extract, 10 g/L tryptone, and 10 g/L sodium chloride. Deionized water serves as the solvent, with the mixed solution adjusted to a pH of 7.4, originating from an initial pH of 7.6. The prepared culture medium undergoes sterilization under conditions of high temperature and pressure (0.1 MPa, 121 °C, 15 min). Upon completion of the sterilization process, 1% of Escherichia coli and Staphylococcus aureus are respectively inoculated into the LB medium. Post-inoculation, the medium is placed in a shaker and incubated in darkness for a period of 24 hours (120 rpm, 30 °C). Seawater specimens were procured from the coastal vicinities of Weihai and Beihai, subsequently filtered through a 0.45 μm acetate fiber membrane to eliminate suspended particulates.

The quantification of viable bacterial populations in the water is executed via the plate counting technique. Upon sample collection, the appropriate dilution ratio is ascertained according to experimental stipulations, followed by a serial dilution of the samples at a factor of ten. A sterilized pipette is then employed to transfer 0.1 mL of the diluted sample, which is meticulously spread over the surface of the cooled culture medium. The coated culture medium is subsequently incubated at a constant temperature of 37 °C for a duration of 24 hours within a biochemical incubator, after which the colonies are enumerated to determine the concentration of viable bacteria present in the water sample.

The efficacy of sterilization is assessed by measuring the concentration of viable bacteria in the

bacterial solution pre- and post-treatment, juxtaposing the number of viable bacteria post-reaction with those present in the untreated water sample. The calculation formula is as follows:

$$\text{Sterilization rate} = \frac{N_0 - N_t}{N_0} \times 100\% \quad (1)$$

In the formula, $N_0$ represents the initial viable cell count prior to treatment, expressed in CFU/mL. Meanwhile, $N_t$ denotes the residual viable bacterial count measured at various time intervals subsequent to a designated duration of treatment, also in CFU/mL.

## 4. Results and Discussion

### *4.1 Design of a biomimetic ER-TENG*

The biomimetic electric ray friction nanogenerator embraces a flexible, planar configuration, allowing it to seamlessly conform to a multitude of curved and irregular surfaces, such as rocks, corals, and sunken vessels on the ocean floor, without necessitating specialized installation or securing apparatus. The incorporation of pliant materials permits the generator to undergo deformation without incurring damage or failure when subjected to external forces. The biomimetic design of electric rays minimizes energy dissipation due to shape incongruence, enhances the contact area and frequency of frictional interactions, and thereby augments the efficiency of energy capture. This adaptable design empowers the nanogenerator to endure dynamic fluctuations in the underwater milieu, including the impact of water currents and subaqueous seismic activities, while maintaining consistent performance. Its flat configuration facilitates easy rolling or folding, rendering transportation and deployment both convenient and efficient.

The operational principle of the biomimetic electric ray friction nanogenerator hinges on the phenomena of triboelectric effect and electrostatic induction (Figure 1). When the surfaces of two disparate materials make contact and subsequently disengage, the variance in their electronegativity induces a transfer of charges, resulting in the accumulation of positive and negative charges on their respective surfaces. These charges generate a potential difference within an external circuit, instigating electron flow and thus producing an electric current. In the biomimetic electric ray friction nanogenerator, these effects are astutely integrated. The generator consists of thin films composed of two distinct materials, engineered into a structure that facilitates repeated contact and separation. Upon contact and separation driven by external forces, the triboelectric effect endows the films with opposing charges. Consequently, these charges establish a potential difference, or voltage, within the external circuit, prompting electron movement and current generation. The efficacy of the biomimetic electric ray generator is significantly influenced by the electronegativity disparities of the chosen materials, the film thickness, and the frequency of contact-separation cycles. By meticulously optimizing these parameters, the generator's output performance and energy conversion efficiency can be markedly enhanced.

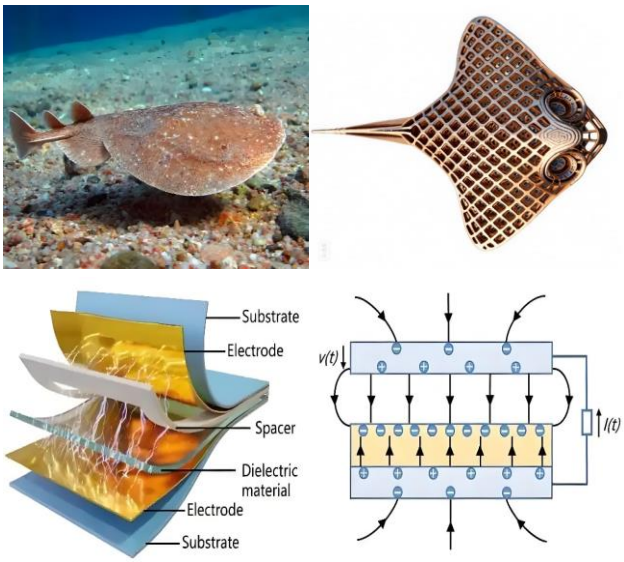


Figure 1: Power generation principle of biomimetic electric ray friction nanogenerator

### *4.2 Mechanism of ER-TENG treatment of ship ballast water*

Seawater serves as a natural electrolyte, comprising an abundant array of salts, predominantly featuring ions such as sodium, magnesium, calcium, chloride, hydrogen, and oxygen. Notably, chloride ions constitute approximately 55% of the total ionic composition. As shown in Figure 2, through the process of electrolysis, utilizing a direct current power source, these chloride ions undergo oxidation to yield chlorine gas. This chlorine gas, once dissolved in seawater, generates potent oxidative

agents capable of microbial eradication, including hypochlorous acid (HClO), hypochlorite ions (ClO-), and sodium hypochlorite (NaClO).

In accordance with the principles of electrolysis, the primary reactions transpiring within the electrolytic cell when seawater is subjected to this process are as follows:

At the anode: $2Cl^- \rightarrow Cl_2 + 2e$ （2）

At the cathode: $2H_2O + 2e \rightarrow 2OH^- + H_2\uparrow$ （3）

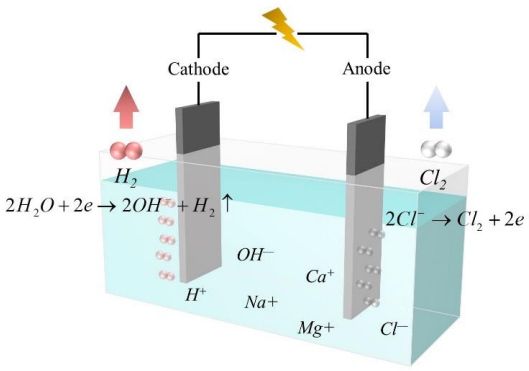


Figure 2: Schematic diagram of the principle of electrolysis of seawater

The electrolytic cell utilized in this experiment, with a capacity of 8000 cm³, is of the diaphragm-free variety. Owing to the high solubility of chlorine gas in water, the anode and cathode solutions within the cell are thoroughly amalgamated, allowing chlorine gas to swiftly engage in a secondary reaction within the solution.

$$Cl_2 + 2OH^- \rightarrow ClO^- + Cl^- + H_2O \quad (4)$$

At a temperature of 25°C, the equilibrium constant $k_c$ for this reaction attains a value of 1.5 × $10^{16}$, signifying a reaction characterized by a high reaction limit. This implies that the reverse reaction can progress nearly to the point of complete conversion. The comprehensive reaction encompassing the aforementioned three reactions is expressed as follows:

$$NaCl + H_2O = NaClO + H_2\uparrow \quad (5)$$

$$Cl_2 + H_2O = HCl + HClO \quad (6)$$

At 25°C, the equilibrium constant *kc* for reaction (6) is 4.2 × $10^{-4}$. In comparison to reaction (4), this reaction exhibits a lower reaction limit and can thus be deemed a secondary reaction.

Hypochlorous acid stands out as the most potent disinfectant among chlorine compounds, with the exception of chlorine dioxide. Additionally, as a weak acid, it is subject to decomposition reactions to a certain extent.

$$HClO = H^+ + ClO^- \quad (7)$$

$$HClO \rightarrow HCl + O \quad (8)$$

In solutions exhibiting pH values spanning from 6.5 to 8.5, hydrogen ions and hypochlorite ions manifest at varying concentrations. The comprehensive data regarding the fluctuation of the ionization constant with temperature is elucidated in Table 1.

Table 1: Values of ionization constants ($K_i$) for *HClO* at different temperatures

| **Temperature /℃** | 0 | 5 | 10 | 15 | 20 | 25 | 30 |
|---|---|---|---|---|---|---|---|
| **$K_i \times 10^8$(mol/L)** | 1.4 88 | 1.7 53 | 2.0 23 | 2.3 20 | 2.6 21 | 2.8 98 | 3.1 75 |

The compounds HClO, $ClO^-$, and $Cl_2$, generated during the reaction, are collectively referred to as effective chlorine. This term serves as an indicator of the disinfectant potency within chloride solutions, owing to their remarkable oxidative and antimicrobial capabilities. HClO and $ClO^-$ are recognized as free and effective chlorine, with their relative proportions being pivotal to their bactericidal efficacy, given that HClO exhibits a bactericidal potential approximately 40 to 80 times greater than that of $ClO^-$. The electrolysis of seawater yields a spectrum of biocidal agents, with effective chlorine encompassing chemical entities characterized by robust oxidative and bactericidal properties, including HClO, $ClO^-$, and $Cl_2$. The production of effective chlorine through the electrolytic process of seawater stands as the fundamental mechanism enabling direct electrochemical disinfection. Within a laboratory setting, these substances permeate the entire system, thereby effectuating the eradication of deleterious aquatic organisms and pathogens.

### *4.3 Effects of Anode Materials on Sterilization Performance*

Under the influence of an external driving

frequency of 1.8 Hz, Figure 3 elucidates the comparative performance of three anode materials-carbon rod, carbon plate, and carbon fiber—in terms of their sterilization efficiency. Upon meticulous analysis of the chart data, it becomes evident that the carbon rod exhibits the highest sterilization efficacy among the anode materials, achieving a remarkable 92.85% inactivation rate within a 15-minute interval. When the carbon plate serves as the anode, the inactivation rate reaches 90.47% at 15 minutes and further ascends to 93.02% at 20 minutes. In contrast, the bactericidal efficacy of carbon fiber is notably inferior to the aforementioned materials, with an inactivation rate of 84.56% at 15 minutes and 89.32% at 50 minutes. After a comprehensive evaluation of the bactericidal capabilities of the three anode materials-carbon rod, carbon plate, and carbon fiber, the findings reveal that the carbon rod possesses the most pronounced bactericidal effect, followed closely by the carbon plate. Given the suboptimal bactericidal performance of carbon fiber relative to the carbon plate, and considering the substantial advantages of the carbon plate in terms of cost-effectiveness and active surface area (when compared to carbon rods of equivalent volume), the carbon plate has been selected as the preferred material for subsequent experimental investigations.

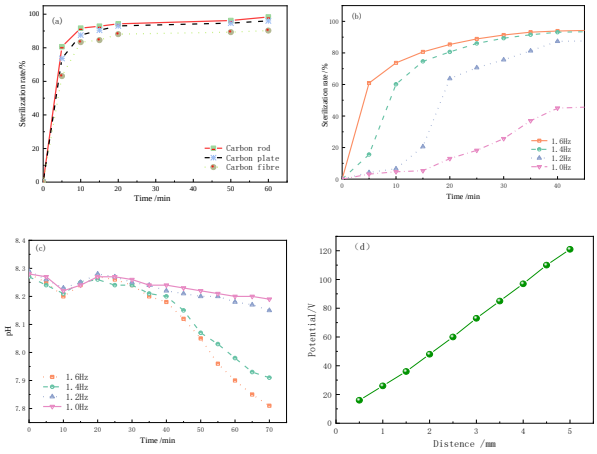


Figure 3: (a) Effect of anode material on sterilization performance; (b) Influence of frequency on sterilization performance; (c) Diagram of the effect of frequency on pH; (d) Relationship between potential and separation distance

### *4.4 Effect of Frequency on Sterilization Performance*

The temporal evolution of sterilization efficacy at various frequencies, utilizing carbon plates as anodes, is depicted in Figure 3(c). At frequencies of 1.0 Hz, 1.2 Hz, 1.4 Hz, and 1.6 Hz, the overall sterilization performance exhibits a consistent upward trajectory over time, with higher frequencies yielding progressively greater sterilization rates. Notably, at 1.6 Hz, the sterilization rate surges from 73.55% at 10 minutes to 94.14% at 60 minutes. Conversely, when the frequency is reduced to 1.4 Hz, the initial rate of sterilization enhancement is markedly slower, achieving 60.11% after 10 minutes of electrolysis and attaining a 94.65% sterilization rate after 40 minutes. At frequencies of 1.2 Hz and 1.0 Hz, the initial phase of sterilization rate improvement is relatively sluggish. After 60 minutes of electrolysis, the sterilization rates reach 87.02% and 46.36%, respectively. Analysis reveals that the suboptimal output performance of the ER-TENG at these two frequencies results in a lower initial oxidation potential at the anode compared to that of chloride ions, thereby hindering the production of chlorine gas and leading to diminished sterilization efficiency in the early stages. However, as the surface charge of the ER-TENG gradually accumulates, its output performance improves, ultimately surpassing the oxidation potential of chloride ions and facilitating the generation of chlorine gas, which exerts its bactericidal effect.

To delve deeper into the mechanisms underlying the sterilization process through electrolytic seawater, this study examined the temporal variations in solution pH under different frequency conditions, as illustrated in Figure 3(d). During the electrolysis process at varying frequencies, the pH value initially declines, subsequently peaks, and then diminishes once more. In the early stages of electrolysis, the chlorine gas produced reacts with seawater to form hydrochloric acid and hypochlorous acid, causing a reduction in the pH value of the seawater. As hypochlorous acid interacts with microorganisms or organic substances and is consumed, the pH value rises to a certain extent. As the electrolysis process progresses and microorganisms or organic matter are increasingly depleted, the pH value reaches a peak before declining anew. By the 70-minute mark of electrolysis, the pH values at frequencies of 1.0 Hz, 1.2 Hz, 1.4 Hz, and 1.6 Hz have decreased to 8.17, 8.10, 7.92, and 7.88, respectively. These findings suggest that as the electrolysis frequency increases,

the quantity of generated chlorine gas also rises, leading to a greater production of $H^+$ ions and a more pronounced decrease in pH value.

*4.5 Steady state calculation*

Upon the establishment of the geometric model and the specification of material parameters, the finite element method (FEM) was employed to discretize the geometric configuration and its surrounding milieu. The mesh was predefined as "finer" and partitioned utilizing a free triangular grid. The grid for the air domain was similarly set to "finer," with cell dimensions ranging from a maximum of 1 mm to a minimum of 0.01 mm. Given the regular rectangular geometry of the copper (Cu) electrode and the polydimethylsiloxane (PDMS) dielectric, a mapped grid was selected to enhance computational precision; the grid size was designated as "ultra-fine," with maximum and minimum cell sizes of 0.05 mm and 0.002 mm, respectively. The mesh discretization in the air is relatively coarse, progressively refining as it approaches the Cu electrode and PDMS.

Employing a steady-state solver in conjunction with the finite element simulation method, and integrating Maxwell's equations, we meticulously simulated and computed the potential distribution across the Cu electrode and PDMS dielectric under varying separations, as depicted in Figure 4. Initially, the Cu electrode maintains complete contact with the PDMS, resulting in a null potential difference due to their electrical connectivity. As the Cu electrode incrementally detaches from the PDMS, an air gap emerges, generating an electric field that facilitates charge transfer among the Cu electrode, PDMS film, and air gap. Consequently, a potential difference materializes between the Cu electrode and the PDMS film, intensifying with the widening gap. Upon reaching a certain maximum separation, the potential difference peaks at 120V, signifying the interval at which the electric field strength and charge transfer are maximized. As the gap narrows from its apex, the potential difference diminishes, attributable to the attenuation of the electric field strength and a concomitant reduction in charge transfer.

In accordance with steady-state analytical research, the interaction between the Cu electrode and PDMS dielectric film reveals remarkable triboelectric and electrostatic induction coupling characteristics. To elucidate the relationship between potential difference and separation distance, simulations were conducted on the potential distribution of the Cu electrode and PDMS film under varying spacing conditions. The findings indicated that with increasing separation distance, the potential difference across the surfaces of the two materials escalates, exhibiting a linear upward trend. A pivotal aspect in executing simulation calculations is the judicious selection of separation spacing, as excessive spacing may amplify edge effects, introducing biases in the computational outcomes. Such deviations can cause the electric field line distribution to mimic the interaction of two-point charges rather than a uniform field distribution. Hence, it is imperative to focus on separation spacing, conducting multiple iterative computations to ascertain the stability and accuracy of the results. Concurrently, other factors potentially influencing the potential distribution, such as material properties, surface morphology, and environmental humidity, must be considered to ensure the comprehensive and reliable nature of the simulation results.

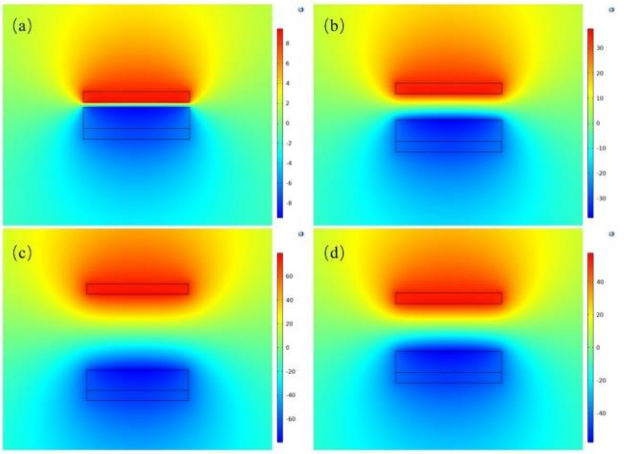


Figure 4: Simulated potential distribution

*4.6 Friction layer output performance test*

The electrical output performance of ER-TENG, composed by integrating a nanocomposite film with copper foil and a PMMA board, was meticulously evaluated. As depicted in Figure 5, the open-circuit voltage of the pristine PDMS-based TENG is measured at 45.21 V, while the short-circuit current registers at 5.27 μA. Notably, the incorporation of $TiO_2$ nanoparticles markedly enhances the electrical output performance of the PDMS-based TENG. This enhancement is attributed to the increase in the

relative dielectric constant of the PDMS nanocomposite film upon the addition of $TiO_2$ nanoparticles, thereby significantly improving its dielectric properties. However, as the concentration of $TiO_2$ nanoparticles is augmented, both the open-circuit voltage and short-circuit current of the TENG exhibit an initial increase followed by a decrease. This phenomenon arises because an elevated $TiO_2$ nanoparticle content diminishes the effective contact friction area of PDMS, leading to a decline in performance after reaching an optimal peak. In the conducted experiment, when the $TiO_2$ nanoparticle doping mass fraction reached 4.25 wt%, the TENG's electrical performance was optimized, achieving a maximum open-circuit voltage of 123.25 V and a peak short-circuit current of 13.52 μA. These values represent enhancements of 2.73 times and 2.56 times, respectively, over the undoped PDMS film. Consequently, in subsequent experiments, a doping mass fraction of 4.65 wt% was selected for PDMS@$TiO_2$ to further investigate the performance of friction nanogenerators utilizing nanocomposite films.

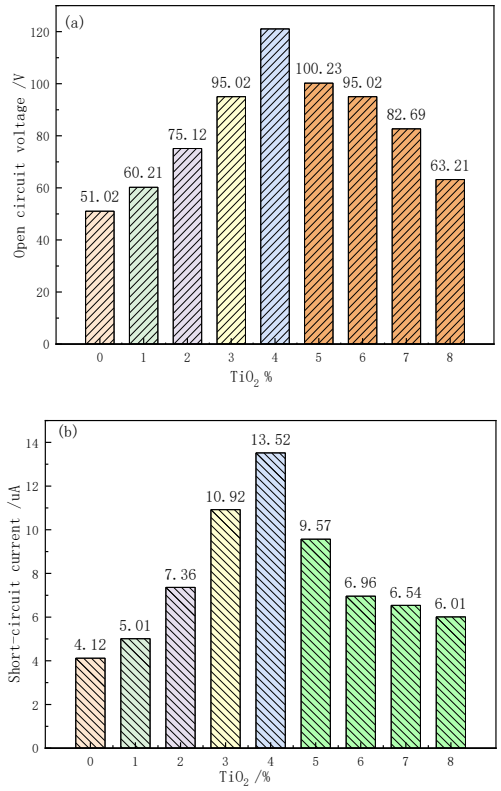


Figure 5: Output voltage for different $TiO_2$ doping concentrations (a); Output current for different $TiO_2$ doping concentrations (b)

## 5. Conclusion

This study investigates the synergy between electrical output performance based on ER-TENG and electrolytic seawater technology for ship ballast water treatment, and delves into the effects of diverse influencing factors on the sterilization efficacy of ballast water treatment. The biomimetic electric ray friction nanogenerator employs a flexible flat design, facilitating its seamless adaptation to various curved and irregular surfaces such as rocks, corals, and sunken ships on the seabed, without necessitating special installation or fixation devices. ER-TENG harnesses blue energy wave energy from the ocean, converting it into electrical energy to fuel electrolysis reactions. The integration of ER-TENG with electrolysis technology for ship ballast water treatment accomplishes efficient mechanical-to-electrical energy conversion, providing stable and sustainable power for electronic devices. The electrical properties of ER-TENG were optimized, yielding a maximum open-circuit voltage of 123.25 V and a peak short-circuit current of 13.52 μA.

Submitted: Nov 26, 2024; Accepted: Nov 27, 2024

## References

[1] Xiao Sun, Liting Dong, Yongjian Liu et al. (2023), Biomimetic PVA-PVDF-based triboelectric nanogenerator with MXene doping for self-powered water sterilization, *Materials Today Nano*, Vol. 24, No. 1, pp. 100410.

[2] Zhong Lin Wang, Guang Zhu, Ya Yang (2012), Progress in nanogenerators for portable electronics, *Materials Today*, Vol. 15, No. 12, pp. 532-543.

[3] Ivana Martić, Nastia Degiuli, Carlo Giorgio Grlj (2024), Scaling of wave energy converters for optimum performance in the Adriatic Sea, *Energy*, Vol. 294, No. 1, pp. 1-12.

[4] Ehsan Kazemi-Robati, Bernardo Silva, Ricardo J. Bessa (2024), Stochastic optimization framework for hybridization of existing offshore wind farms with wave energy and floating photovoltaic systems, *Journal of Cleaner Production*, Vol. 454, No. 1, pp. 142215.

[5] Alfredo Sánchez, Edgar Mendoza (2024), Wave energy converter farm feasibility assessment in southwest Baja California, Mexico, *Renewable Energy*, Vol. 227, No. 1, pp. 120589.

[6] Jinlong Ren, Liyang Fang, Hang Qu (2024), A wave-powered capacitive deionization system with in-situ blue

energy harvester, *Chemical Engineering Journal*, Vol. 498, No. 1, pp. 155530.

[7] He Li, Zhen Zhang, Peng Xu (2024), A vortex-induced vibration device based on MG-TENG and research of its application in ocean current energy harvesting, *Nano Energy*, Vol. 124, No. 1, pp. 109457.

[8] Ying Lou, Mengfan Li, Jiaxi Hu (2024), Maximizing the energy conversion of triboelectric nanogenerator through the synergistic effect of high coupling and dual-track circuit for marine monitoring, *Nano Energy*, Vol. 121, No. 1, pp. 109240,

[9] Shuqin Zhang, Wenpo Li, Gui Li et al. (2024), High performance DC-TENG based on coupling of mismatched number of triboelectric units and electrodes with mechanical switches for metal surface anti-corrosion, *Nano Energy*, Vol. 130, No. 1, pp. 110093.

[10] Shaojun Zhang, Zhirao Yin, Qianyong (2024), Simulation of Self-Powered Electric-Eel Friction Nanogenerator, *Procedia Computer Science*, Volume 243, 2024, pp. 734-743.

[11] Mohamed Salman, Vladislav Sorokin, Kean Aw. (2024), Systematic literature review of wave energy harvesting using triboelectric nanogenerator, *Renewable and Sustainable Energy Reviews*, Vol. 201, pp. 114626.

[12] Kushal Ruthvik Kaja, Sugato Hajra, Swati Panda et al. (2024), Exploring liquid-solid interface based triboelectrification, structures, and applications, *Nano Energy*, Vol. 131, No. 1, Part B, pp. 110319.

[13] Ming Yuan, Wenlong Zhang, Yanhang Tai (2024), Tympanic membrane metamaterial inspired multifunctional low-frequency acoustic triboelectric nanogenerator, *Nano Energy*, Vol. 128, No. 1, Part A, pp. 109816.

[14] Hao Wu, Runze Rao, Hengyu Guo (2024), Research on performance of solid-liquid triboelectric nanogenerators based on anti-rolling tank, *Applied Energy*, Vol. 353, No. 1, Part B, pp. 122153.

[15] Arunkumar Chandrasekhar, Sayyid Abdul Basith, Venkateswaran Vivekananthan et al. (2024), Smart maracas: An innovative triboelectric nanogenerator for earthquake detection and energy harvesting, *Nano Energy*, Vol. 123, No. 1,pp. 109379.

[16] Leonardo Romero-Martínez, Cees van Slooten, Michiel van Harten et al. (2024), Comparative assessment of four ballast water compliance monitoring devices with natural UV-treated water using IMO's monitoring approaches, *Marine Pollution Bulletin*, Vol. 209, No. 1, Part B, 2024, pp. 117193.

[17] Isabelle D. de Oliveira, Eduardo Ferreira-Machado, Jamile M. Garcia et al. (2024), Disseminated paracoccidioidomycosis in a captive western black-handed tamarin (Saguinus niger), *Journal of Comparative Pathology*, Vol. 214, No. 1: pp. 1-6.

**Received** **11 November 2024**

**1st Revised** **19 December 2024**

**Accepted** **23 December 2024**